Electronic Supplementary Information

Experimental section

Materials: Niobium oxalates (purity, 99.95%), oxalic acid, sodium sulfate, and ethanol were obtained from Aladdin Ltd. (Shanghai, China). CC was purchased from Hongshan District, Wuhan Instrument Surgical Instruments business. Salicylic acid, ammonium chloride, *p*-dimethylaminobenzaldehyde, sodium citrate dehydrate, sodium nitroferricyanide dihydrate, and sodium hypochlorite solution were purchased from Beijing Chemical Corp. (China). Ultrapure water used throughout all experiments was purified through a Millipore system. All the reagents were used as received without further purification.

Preparation of Nb_2O_5/CC: Typically, 1.07 g niobium oxalates (2 mmol) and 1.13 g oxalic acid (9 mmol) was mixed in 40 mL deionized water. Then, the solution was heated to 80°C for 20 min with stirring. After that, a piece of CC (2 cm × 2 cm) was immersed into the solution and was transferred into a 50 ml Teflon-lined autoclave. The autoclave was sealed and heated at 180 °C for 12 h in an electric oven. Finally, the obtained material was washed and dried.

Preparation of Nb_2O_5/CP: First, 5 mg Nb_2O_5 powder and 20 μL of Nafion solution (5 wt%) were dispersed in 980 μL mixed solution contain ethanol and H_2O (V:V=2:1) by 0.5 h sonication to form a homogeneous ink. Then 20 μL catalyst ink was loaded on a 1 × 1 cm^2 CP and dried under ambient condition for measurement.

Characterizations: XRD patterns were obtained from a Shimazu XRD-6100 diffractometer with Cu Kα radiation (40 kV, 30 mA) of wavelength 0.154 nm (Japan).

SEM images were collected from the tungsten lamp-equipped SU3500 scanning electron microscope at an accelerating voltage of 20 kV (HITACHI, Japan). TEM images were obtained from a Zeiss Libra 200FE transmission electron microscope operated at 200 kV. XPS measurements were performed on an ESCALABMK II X-ray photoelectron spectrometer using Mg as the exciting source. The absorbance data of spectrophotometer were measured on SHIMADZU UV-1800 ultraviolet-visible (UV-Vis) spectrophotometer. A gas chromatograph (SHIMADZU, GC-2014C) equipped with MolSieve 5A column and Ar carrier gas was used for H_2 quantifications. Gas-phase product was sampled every 1000 s using a gas-tight syringe (Hamilton).The data of ion chromatography were measured on Swiss Wang tong ECO.

Electrochemical measurements: The electrochemical performance measurement was performed in a two-compartment cell separatedby Nafion membrane using a CHI 660E station. Before NRR test, Nafion membrane was protonated by boiling in water for 1 h, then in H_2O_2 for 1 h, then in water for another hour, followed by 3 h in 0.5 M H_2SO_4, and finally for 6 h in water. All steps were performed at 80°C. TheNb_2O_5/CC was used as the working electrode (0.4 cm × 0.5 cm), a graphite rod as the counter electrode and Ag/AgCl electrode as the reference. Before the NRR measurements, the Na_2SO_4 electrolyte (0.1 M) was bubbled with N_2 for 20 min. All experiments were carried out at room temperature (~25 °C). The presented current density was referred to the geometrical area of the CC. For N_2 reduction experiments, potentiostatic test was conducted in N_2-saturated 0.1 M Na_2SO_4 solution. N_2 was continuously fed into the cathodic compartment with a properly positioned sparger during the experiments. The

potentials reported in this work were converted to reversible hydrogen electrode (RHE) scale via calibration with the following equation: in 0.1 M Na_2SO_4 aqueous solution, E (vs. RHE) = E (vs. Ag/AgCl) + 0.059 × pH + 0.197 V.

Determination of NH_3: NH_3 concentration was detected by salicylic acid analysis method using UV-Vis spectrophotometry. In detail, 4 mL electrolyte was obatined from the cathodic chamber and mixed with 50 μL oxidizing solution containing NaClO (ρCl = 4 ~ 4.9) and NaOH (0.75 M), 500 μL coloring solution containing 0.4 M $C_7H_6NaO_3$ and 0.32 M NaOH, and 50 μL catalyst solution (1 wt% $Na_2[Fe(CN)_5NO]$) for 2 h. Absorbance measurements were performed at λ=660 nm. The concentration-absorbance curve was calibrated using standard NH_4Cl solution with NH_3 concentrations of 0.0, 0.1, 0.2, 0.3, 0.4, 0.5, and 0.6 μg mL^{-1} in 0.1 M Na_2SO_4. Typically, 500 μg mL^{-1} NH_3 solution was prepared (0.79g NH_4Cl dissolved in 500 ml deionized water) and diluted to 5 μg mL^{-1}. Then, 0.0, 0.2, 0.4, 0.6, 0.8, 1.0, 1.2 mL NH_3 solution with concentration of 5 μg mL^{-1} were poured into 10 mL test tubes and separately diluted to 10 mL with 0.1 M Na_2SO_4 and the resulting concentrations of NH_3 in the solutions are 0.0, 0.1, 0.2, 0.3, 0.4, 0.5, and 0.6 μg mL^{-1}. The fitting curve ($y=0.66x+0.02$, $R^2=0.999$) shows good linear relation of absorbance value with NH_3 concentration by three times independent calibrations.The NH_3 concentration was calculated from the calibration curve,and the rate of NH_3 yield was calculated using the following equation:

NH_3 yield = $(c_{NH3} \times V) / (17 \times t \times A)$

where c_{NH3} is the measured NH_3 concentration, V is the volume of electrolyte, t is the reduction reaction time and A is the geometric area of the cathode (0.4 cm × 0.5 cm).

Determination of FE: Assuming three electrons were needed to produce one NH_3 molecule, the FE in 0.1 M Na_2SO_4 could be calculated as follows:

$FE = 3F \times c_{NH3} \times V / 17 \times Q$

Where F is the Faraday constant, Q is the quantity of applied electricity.

Determination of N_2H_4: The concentration of N_2H_4 was prepared as follows. Firstly, 2 mg mL^{-1} N_2H_4 solution was prepared and diluted to 2 μg mL^{-1}. Then, 0.0, 0.5, 1.0, 1.5, 2.0, 2.5, 5.0 mL N_2H_4 solution with concentration of 2 μg mL^{-1} were poured into 10 mL test tubes and separately diluted to 5 mL with 0.1 M Na_2SO_4 and the resulting concentrations of N_2H_4 in the solutions are 0.0, 0.2, 0.4, 0.6, 0.8, 1.0, 2.0 μg mL^{-1}. The N_2H_4 present in the electrolyte was determined by the method of Watt and Chrisp. Thep-$C_9H_{11}NO$ (5.99 g), 0.1 M Na_2SO_4 (30 mL), and C_2H_5OH (300 mL) were mixed and used as a color reagent. In detail, 5 mL electrolyte was removed from the electrochemical reaction vessel, and added into 5 mL prepared color reagent and stirred 15 min at 25 °C. The obtained calibration curve of N_2H_4 is Y=0.366 X + 0.053, R^2=0.999.

Calculation of ECSA: Electrochemical capacitance measurements were used to determine the active surface area of Nb_2O_5/CC. To measure the electrochemical capacitance, the potential was swept between –0.41 to –0.51 V with scanning rates of 20, 40, 60, 80, 100, and 120 mV s^{-1}, respectively. The specific capacitance can be converted into an ECSA using the specific capacitance value for a flat standard with 1

cm^2 of real surface area. The specific capacitance for a flat surface is generally found to be in the range of 20−60 μF cm^{-2}. In the following calculations of TOF we assume 60 μF cm^{-2}.

ECSA calculation:

$$A_{ECSA}^{Nb_2O_5} = \frac{701\ \mu F\ cm^{-2}}{60\ \mu F\ cm^{-2} per\ cm_{ECSA}^2} = 11.68\ cm_{ECSA}^2$$

TOF calculation:

$$TOF = \frac{NH_3\ yield \times geometric\ area \times 17 \times N_A}{surfacs\ sites \times A_{ECSA}}$$

Since the exact nitrogen binding sites are not known, we conservatively estimate the number of active sites as the total number of surface sites (only Nb atoms as possible active sites) from the roughness factor together with the unit cell of the Nb_2O_5 (Fig. S19).

Surface sites per real surface area:

$$Surfaces\ sites = \left(\frac{Atoms\ per\ unit\ cell}{Volume/unit\ cell}\right)^{\frac{2}{3}} = 8.26 \times 10^{14}\ atoms\ cm_{real}^{-2}$$

Calculation Details: DFT-based first-principles calculations were performed with the generalized gradient approximation (GGA)[1] in the form of the Perdew, Burke, and Ernzerhof (PBE)[2] exchange-correlation functional, as implemented in the Dmol[3] package.[1,3] Geometry optimization was performed using a six atom layers Nb_2O_5 (001) surface with 20 Å vacuum space to avoid the interaction form nearby layers. Layers 1 to 2 are surface layers, layers 3 to 6 are central layers. All atoms were fully relaxed until the convergence criteria for energy were set to be 10^{-5} eV, and the residual forces on each atom became smaller than 0.002 Ha $Å^{-1}$. The N_2 dissociation minimum energy

path (MEP) was obtained by LST/QST tools in DMol^3 code.[4] The Brillouin zone integration was performed with 1 × 2 × 1 Γ-centred Monkhorst-Pack k-point meshes in geometry optimization. Frequencies of each complex were calculated after geometry optimization, and the free energy was obtained as follows:

$$\Delta G=\Delta E+\Delta ZPE-T\Delta S+\Delta G_u$$

where ΔE is the difference in DFT-calculated total energy change, ΔZPE and ΔS are the difference in zero-point energy and the change in entropy between the products and reactants, respectively. T is the temperature (298.15 K), $\Delta G_U = -neU$, where U is the electrode potential with respect to the normal hydrogen electrode, and *n* is the number of transferred charge. The N_2 adsorption energy is defined asfollows:

$$E_{ads} = E_{N_2/substrate} - E_{substrate} - E_{N2}$$

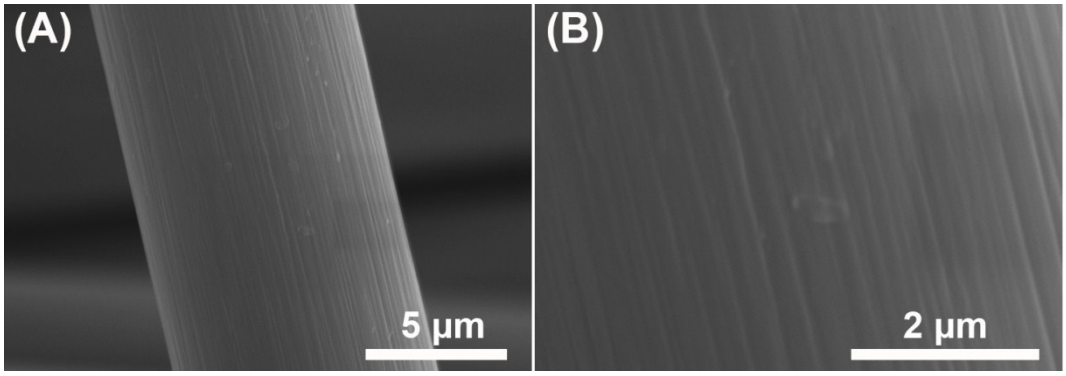

Fig. S1. SEM images of bare CC.

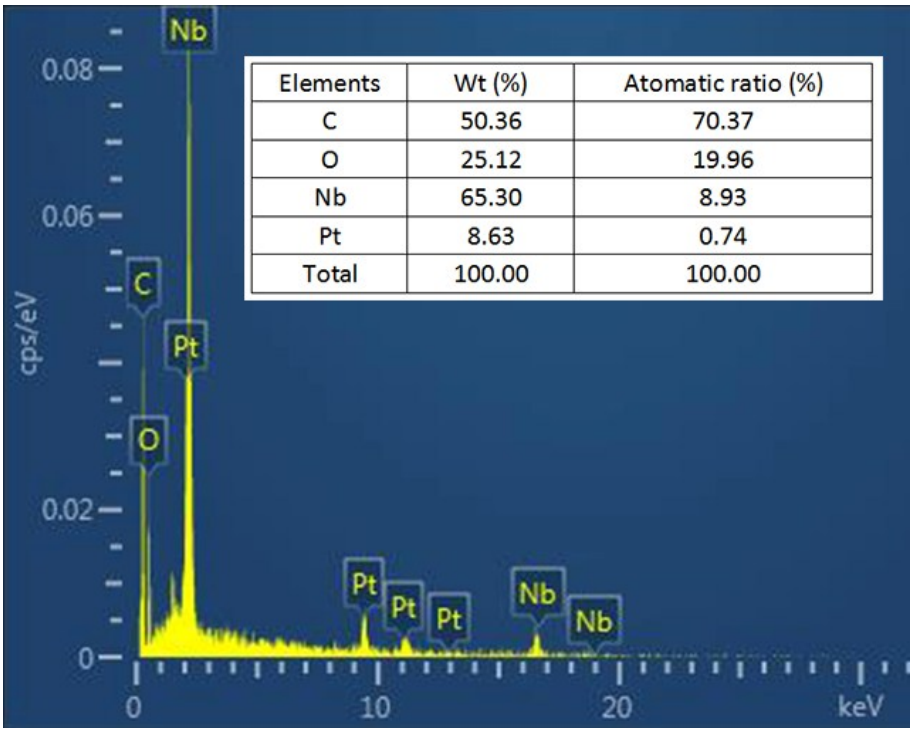

Elements	Wt (%)	Atomatic ratio (%)
C	50.36	70.37
O	25.12	19.96
Nb	65.30	8.93
Pt	8.63	0.74
Total	100.00	100.00

Fig. S2. EDX spectrum ofNb_2O_5/CC.

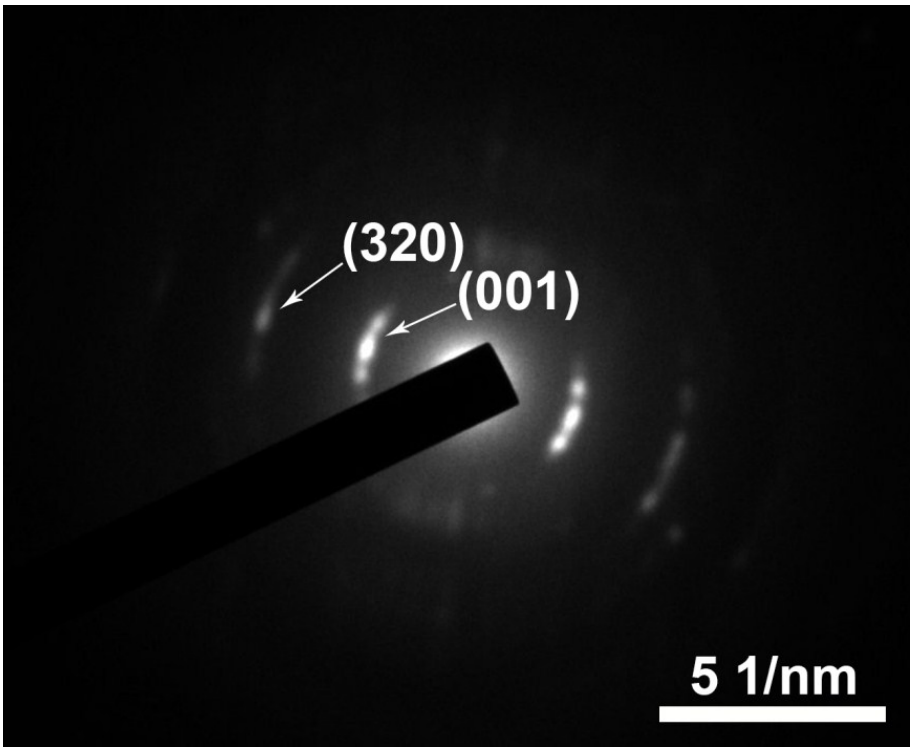

Fig. S3. SAED pattern takenfrom Nb_2O_5nanowires.

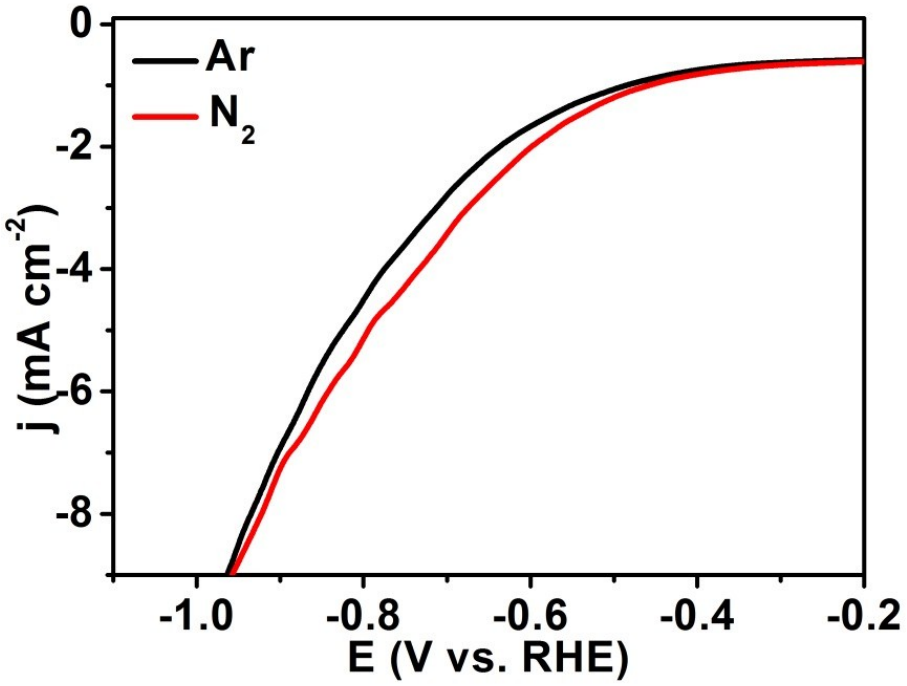

Fig. S4. LSV curves of Nb_2O_5/CC in Ar- and N_2-saturated 0.1 M Na_2SO_4 with a scan rate of 5 mV s^{-1}.

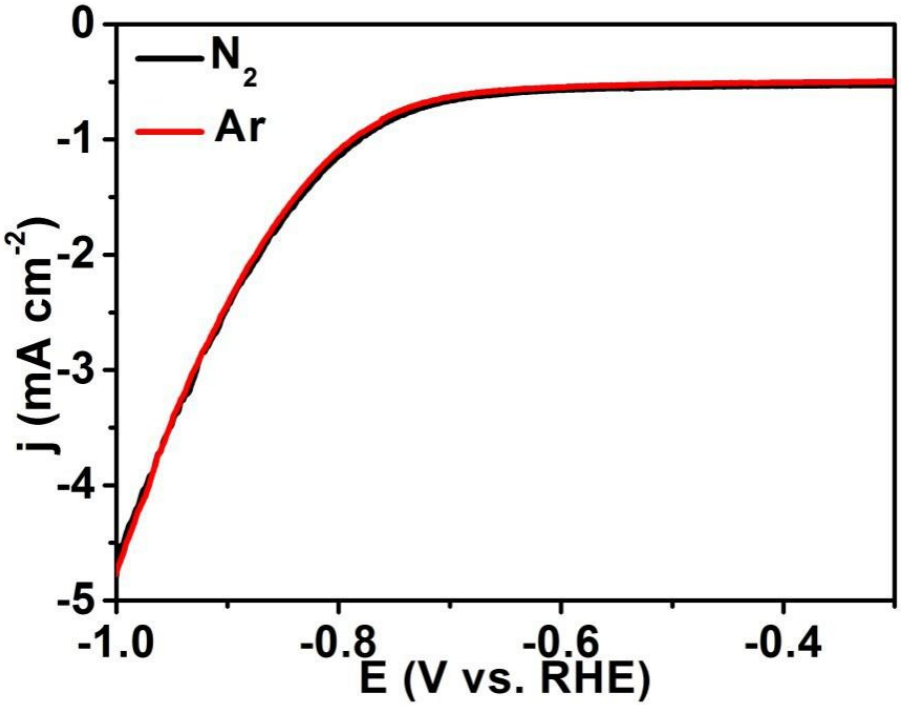

Fig. S5. LSV curves of bare CC in Ar- and N_2-saturated 0.1 M Na_2SO_4 with a scan rate of 5 mV s^{-1}.

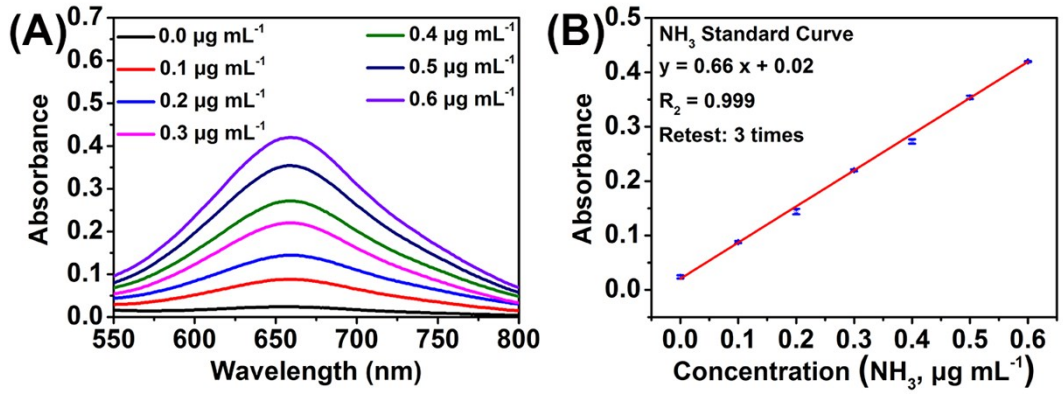

Fig. S6. (A) UV-Vis absorption spectra of various NH_3 concentrations after incubated for 2 h at room temperature. (B) Calibration curve used for calculation of NH_3 concentrations.

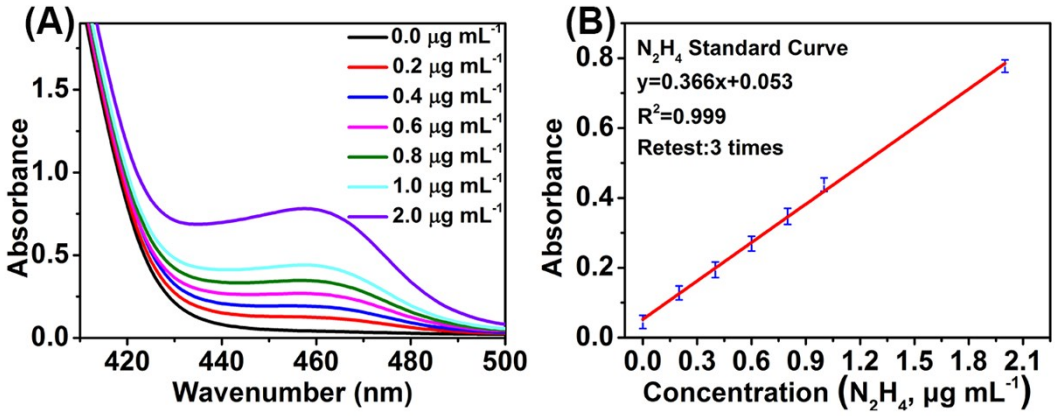

Fig. S7. (A) UV-Vis absorption spectra of various N_2H_4 concentrations after incubated for 15 min at room temperature. (B) Calibration curve used for estimation of N_2H_4 concentrations.

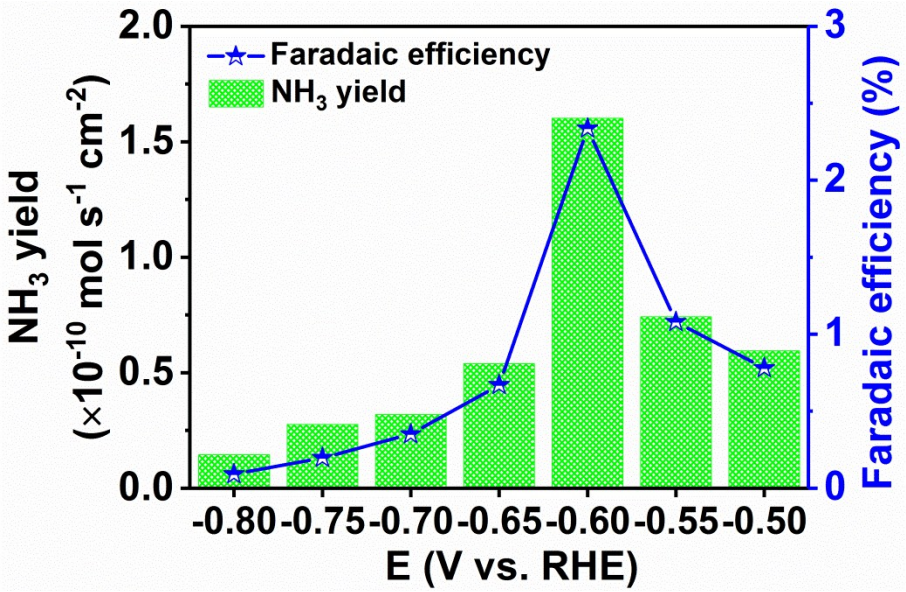

Fig. S8. NH_3 yields and FEs for Nb_2O_5/CC at a series of potentials for 10000 s obtained by Ion chromatography.

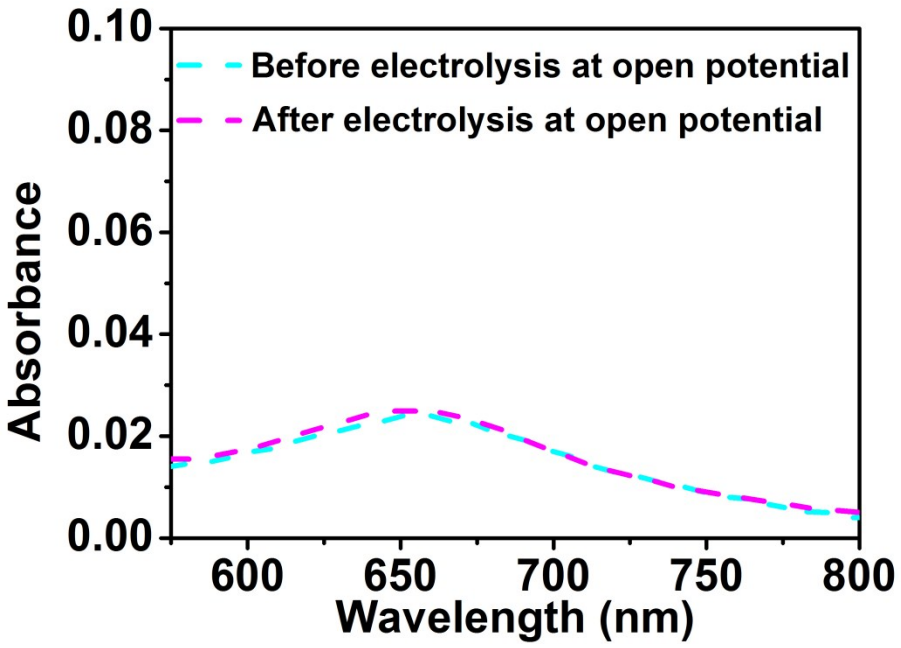

Fig. S9. UV-Vis spectra of the electrolyte stained with indophenol indicator before and after 10000s electrolysis at open potential in N_2-saturated solution.

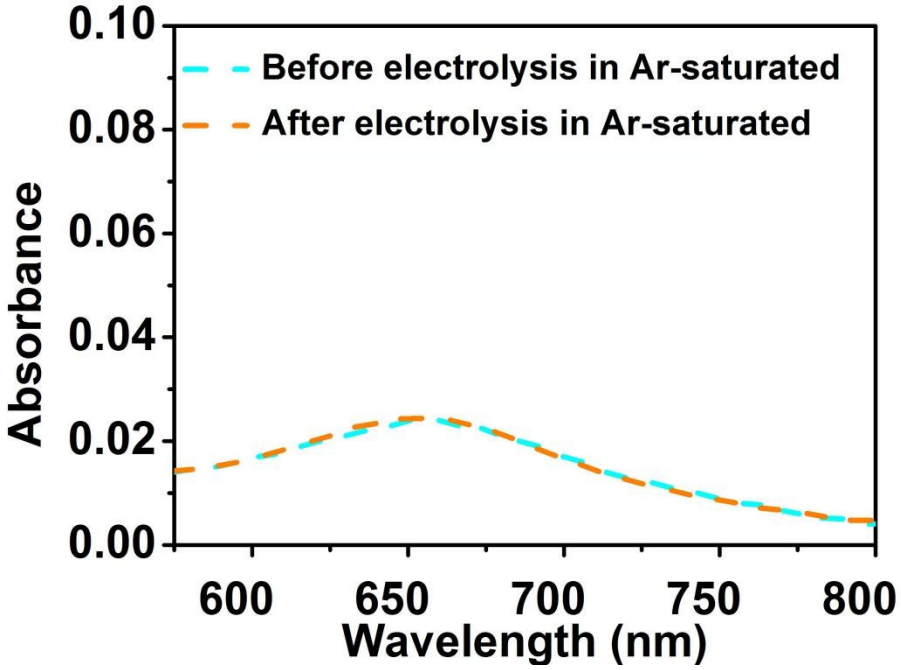

Fig. S10. UV-Vis spectra of the electrolyte stained with indophenol indicator before and after 10000 s electrolysis at the potential of -0.60 V in Ar-saturated solution on Nb_2O_5/CC.

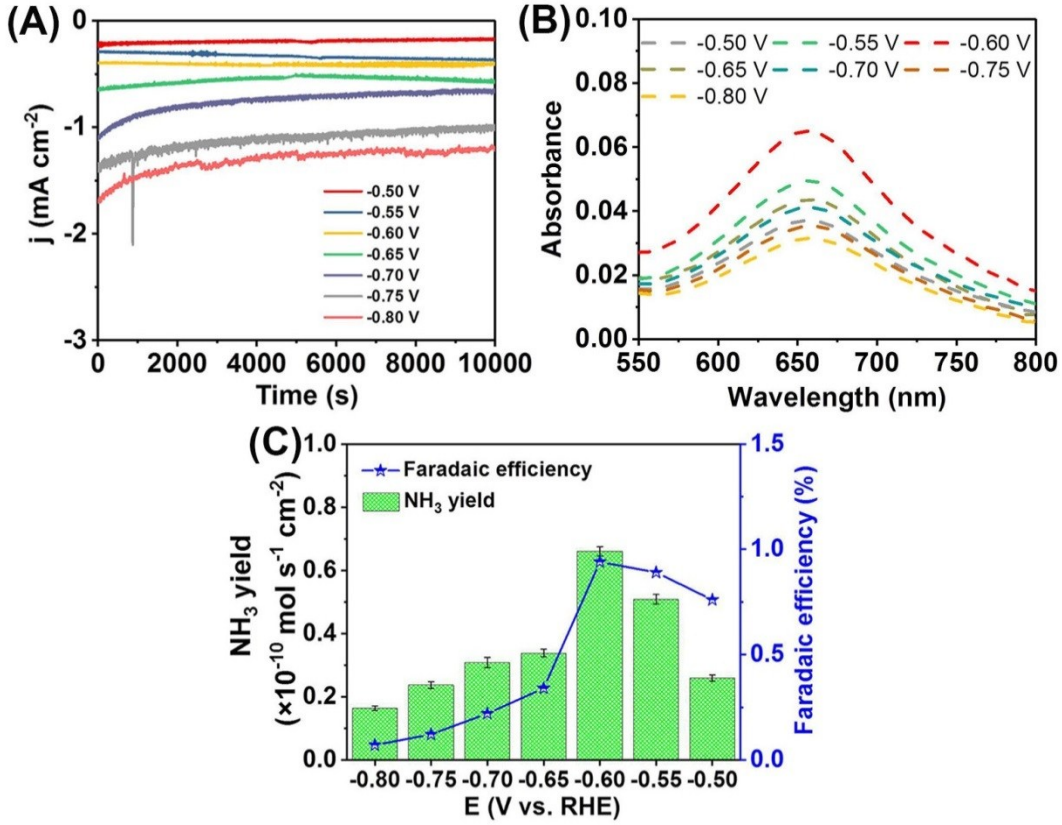

Fig. S11. (A) Time-dependent current density curves for Nb_2O_5/CP at different potentials in 0.1 M Na_2SO_4. (B) UV-Vis absorption spectra of the 0.1 M Na_2SO_4 electrolytes stained with indophenol indicator after electrolysis at a series of potentials. (C) NH_3 yields and FEs at each given potential.

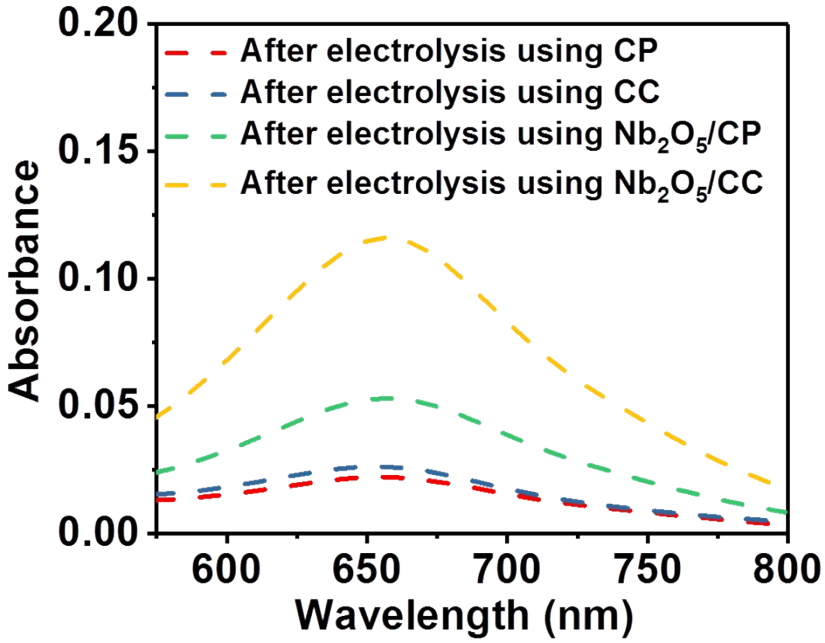

Fig. S12. UV-Vis spectra of the electrolyte stained with indophenol indicator after 10000 s electrolysis in N_2-saturated solution at the potential of -0.60 V using bare CP, bare CC, Nb_2O_5/CP and Nb_2O_5/CC as the working electrode,respectively.

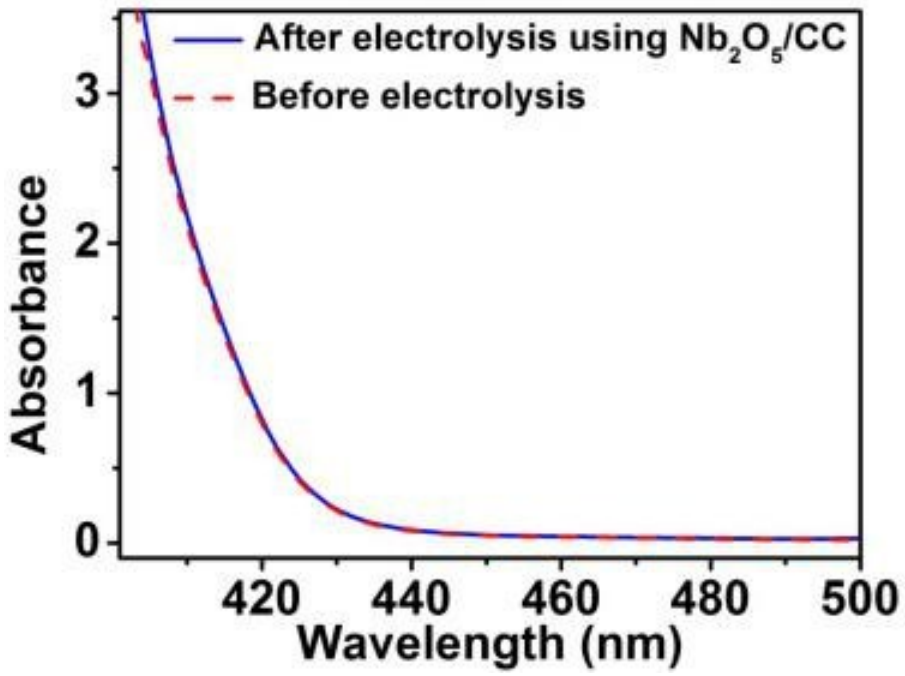

Fig. S13. UV-Vis absorption spectra of the electrolytes estimated by the method of Watt and Chrisp before and after 10000 s electrolysis in N_2-saturated solution at –0.60 V.

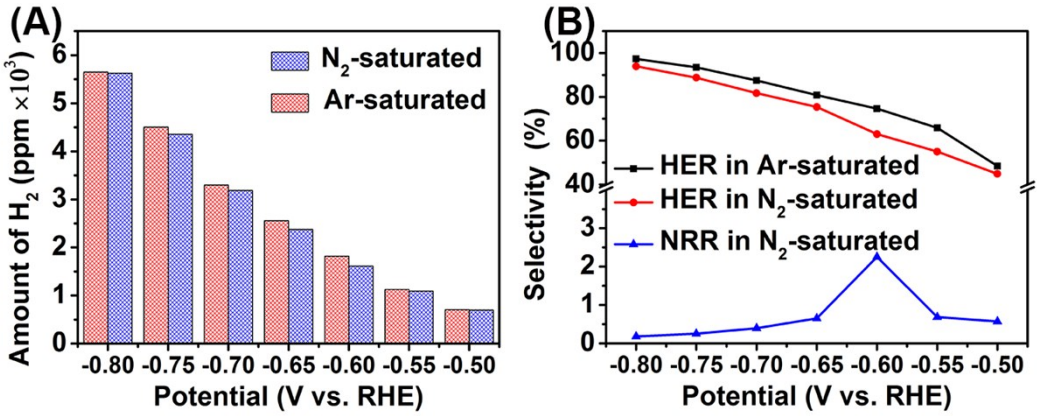

Fig. S14. (A) Comparison of the amounts of H_2 determined by gas chromatography from the headspace of the cell in Ar- and N_2-saturated solution at various potentials. (B) The calculated HER and NRR selectivity.

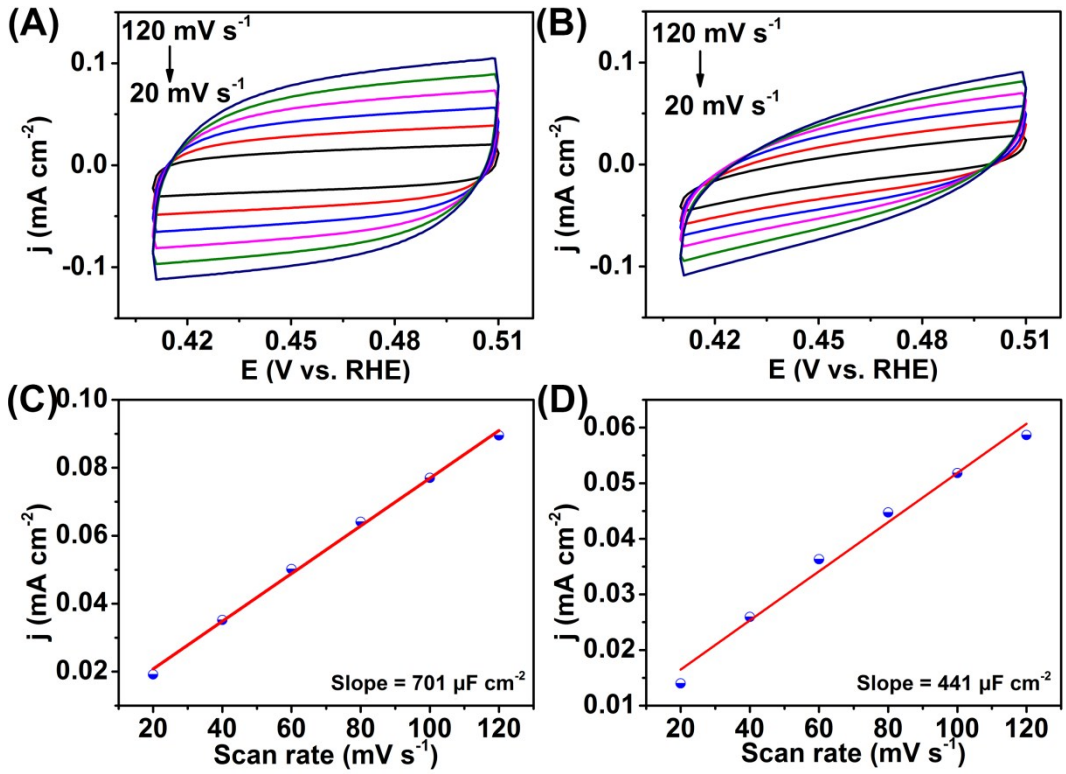

Fig. S15. CVs for (A) Nb_2O_5/CC and (B) bare CC in the non-faradaic capacitance current range at scan rates of 20, 40, 60, 80, 100, and 120 mV s^{-1}. Corresponding capacitive currents at 0.46 V as afunction of scan rate for (C) Nb_2O_5/CC and (D) bare CC in 0.1 M Na_2SO_4, respectively.

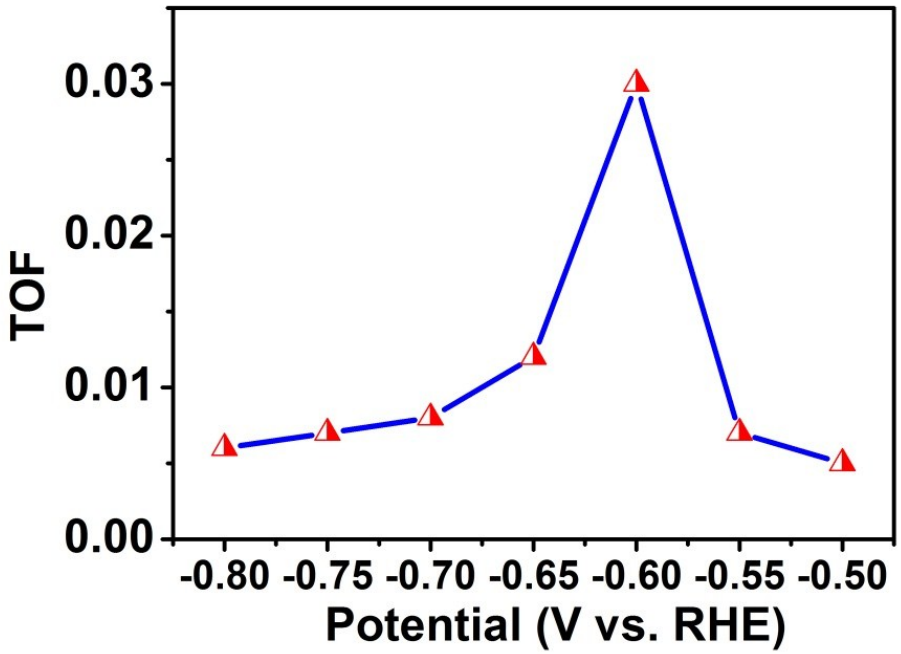

Fig. S16. Plot of TOF vs. potential for Nb_2O_5/CC.

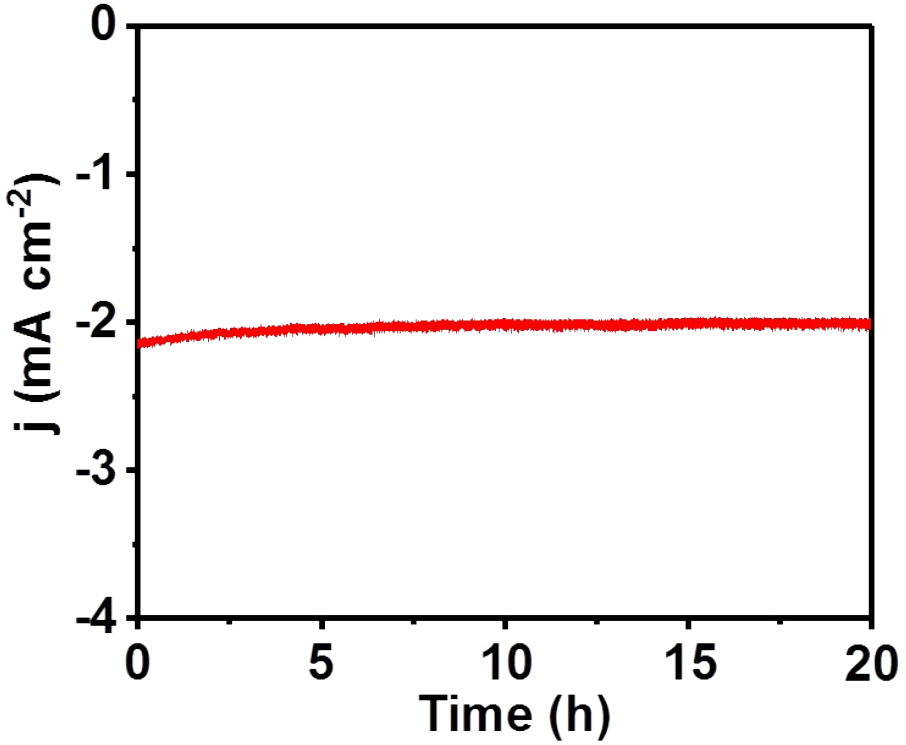

Fig. S17. Chrono-amperometry curve at potential of −0.60 V using Nb_2O_5/CC catalyst.

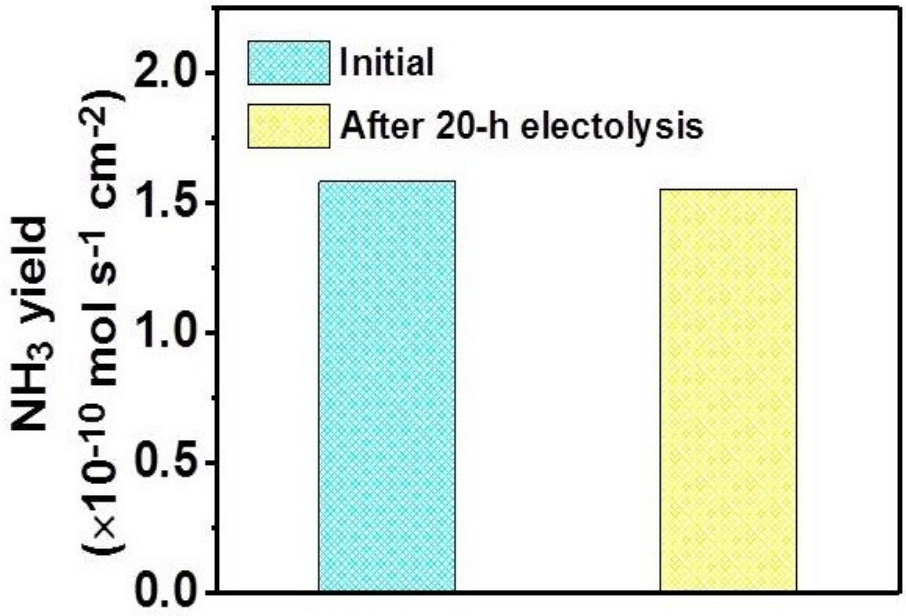

Fig. S18. NH_3 yield rates of Nb_2O_5/CC after charging at －0.60 V for 10000 s (initial) and 20 h.

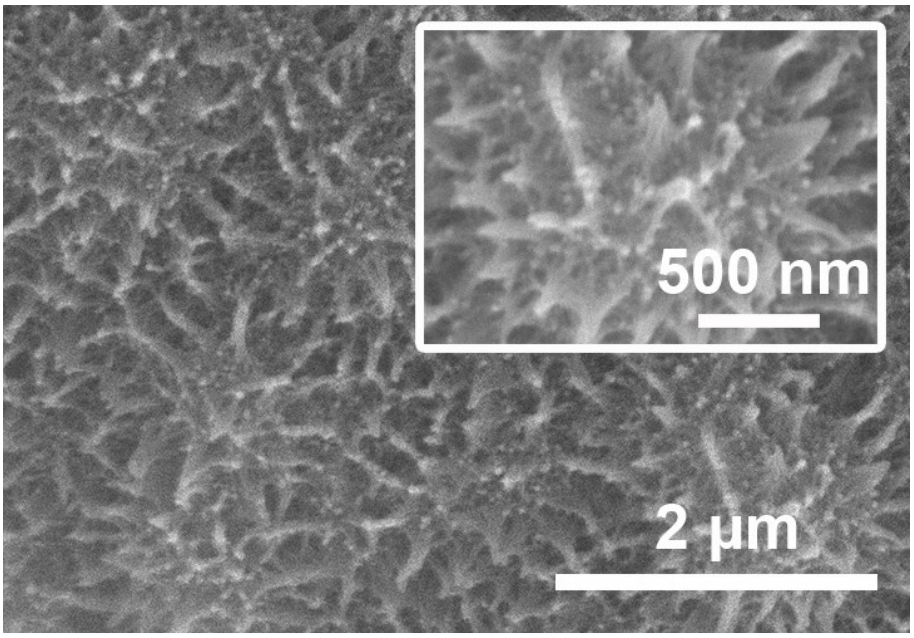

Fig. S19. SEM images of Nb_2O_5/CC after stability test in 0. 1 M Na_2SO_4.

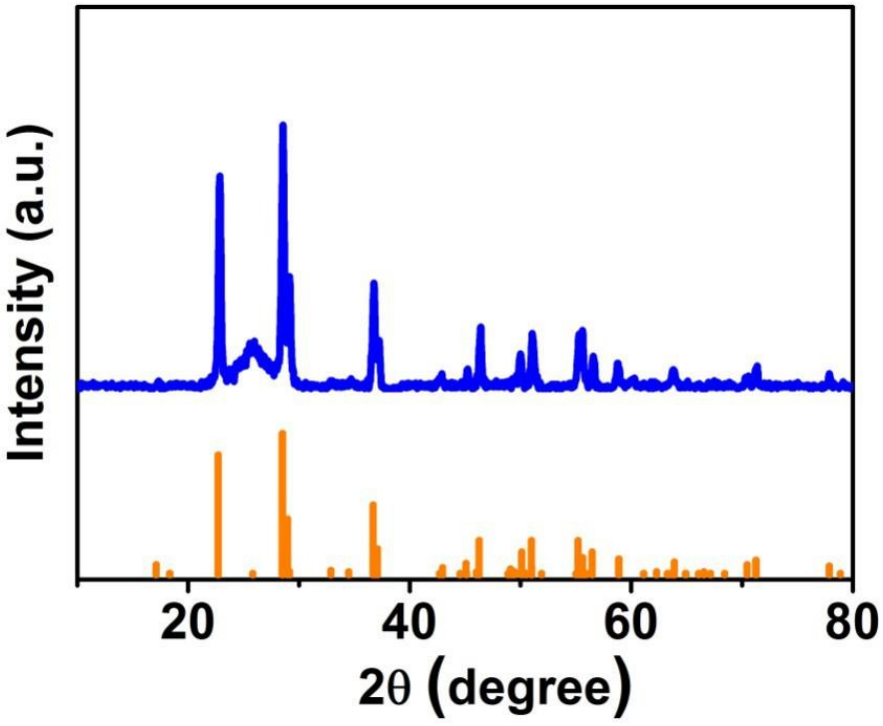

Fig. S20. XRD pattern for Nb_2O_5/CC after stability test in 0.1 M Na_2SO_4.

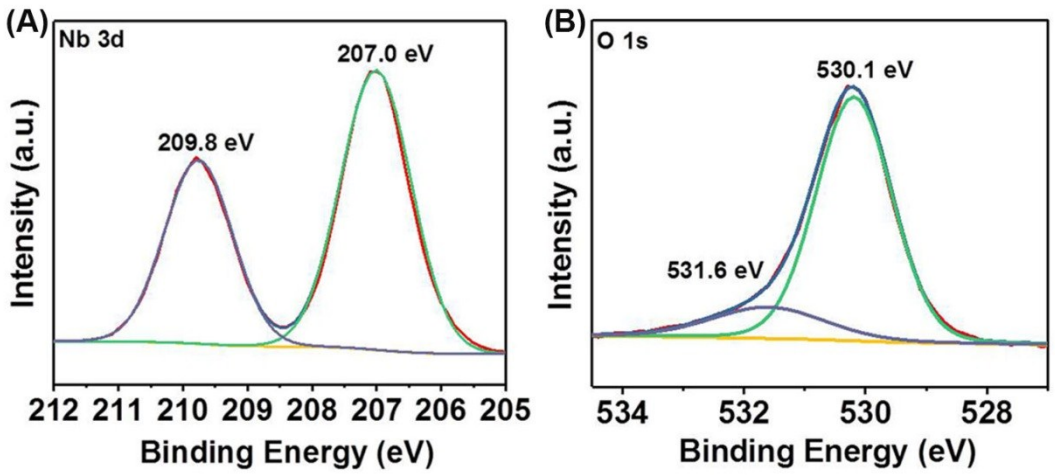

Fig. S21. XPS spectra for Nb_2O_5/CC after stability test in the (A) Nb 3d and (B) O 1s regions.

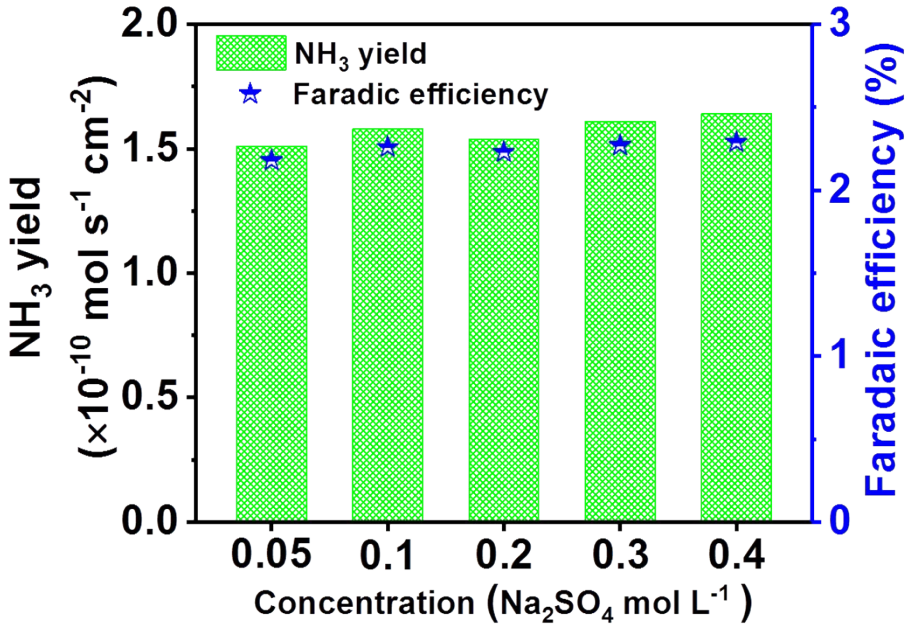

Fig. S22. NH_3 yields and FEs of Nb_2O_5/CC with different electrolyte concentrations.

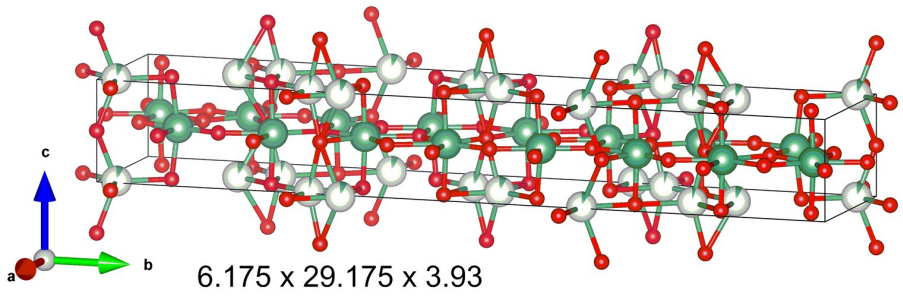

Fig. S23. Nb_2O_5 unit cell.

Table S1. Comparison of theNH_3 electrosynthesis activity for Nb_2O_5/CC with other catalysts.

Catalyst	Electrolyte	NH_3 yield rate	FE (%)	Ref.
Nb_2O_5/CC	0.1 M Na_2SO_4	1.58×10^{-10} mol $s^{-1}cm^{-2}$ 17.63 μg $h^{-1}mg^{-1}_{cat.}$	2.26	This work
Fe_2O_3-CNT	$KHCO_3$	3.58×10^{-12}mol $s^{-1}cm^{-2}$	0.15	5
Fe_3O_4/Ti	0.1 M Na_2SO_4	5.60×10^{-11} mol s^{-1} cm^{-2}	2.60	6
Fe/Fe_3O_4	0.1 M PBS	3.10×10^{-12} mol s^{-1} cm^{-2}	8.29	7
Fe_2O_3 nanorods	0.1 M Na_2SO_4	15.9 μg $h^{-1}mg^{-1}_{cat.}$	0.94	8
PEBCD/C	0.5 M Li_2SO_4	2.58×10^{-11} mol s^{-1} cm^{-2}	2.85	9
MoS_2/CC	0.1 M Na_2SO_4	8.08×10^{-11}mol $s^{-1}cm^{-2}$	1.17	10
defect-rich MoS_2 nanoflower	0.1 M Na_2SO_4	29.28 μg h^{-1} $mg^{-1}_{cat.}$	8.34	11
TiO_2	0.1 M Na_2SO_4	9.16×10^{-11}mol s^{-1} cm^{-2}	2.50	12
TiO_2-rGO	0.1 M Na_2SO_4	15.13 μg $h^{-1}mg^{-1}_{cat.}$	3.3	13
hollow Cr_2O_3 microspheres	0.1 M Na_2SO_4	25.3 μg $h^{-1}mg^{-1}_{cat.}$	6.78	14
C-TiO_2	0.1 M Na_2SO_4	16.22 μg h^{-1} $mg^{-1}_{cat.}$	1.84	15
MnO	0.1 M Na_2SO_4	1.11×10^{-10} mol s^{-1} cm^{-2}	8.02	16
Mn_3O_4 nanocube	0.1 M Na_2SO_4	11.6 μg h^{-1} $mg^{-1}_{cat.}$	3.0	17
SnO_2	0.1 M Na_2SO_4	1.47×10^{-10} mol s^{-1} cm^{-2}	2.17	18
Porous bromide-derived Ag film	0.1 M Na_2SO_4	2.07×10^{-11} mol s^{-1} cm^{-2}	7.36	19
Boron-doped TiO_2	0.1 M Na_2SO_4	14.4 μg h^{-1} $mg^{-1}_{cat.}$	3.4	20

Table S2. Data obtained from the Ion chromatography for NH4+ concentrations after electrolysis for 10000s at a series of potentials.

Sample	Potential (V vs. RHE)	Concentration (NH_4^+, mg L^{-1})
1	–0.50	0.0729
2	–0.55	0.0908
3	–0.60	0.1961
4	–0.65	0.0659
5	–0.70	0.0391
6	–0.75	0.0337
7	–0.80	0.0177

Table S3. ECSA and mass normalized NH_3 yield rates.

Potential (V)	Yield rate (GSA) (mol s^{-1} cm^{-2})	Yield rate (ECSA) (mol s^{-1} cm_{ECSA}^{-2})	Yield rate (Mass) ($\mu g h^{-1} mg^{-1}_{cat.}$)
–0.50	2.31×10^{-11}	1.97×10^{-12}	2.57
–0.55	3.63×10^{-11}	3.11×10^{-12}	4.04
–0.60	1.58×10^{-10}	1.36×10^{-11}	17.63
–0.65	5.61×10^{-11}	4.80×10^{-12}	6.24
–0.70	4.12×10^{-11}	3.53×10^{-12}	4.59
–0.75	3.31×10^{-11}	2.82×10^{-12}	3.67
–0.80	2.81×10^{-11}	2.40×10^{-12}	3.12

References

1 B. Delley, *J. Chem. Phys*., 1990, **92**, 508–517.

2 J. P. Perdew, K. Burke and M. Ernzerhof, *Phys. Rev. Lett.*, 1996, **77**, 3865.

3 B. Delley, *J. Chem. Phys*., 2000, **113**, 7756–7764.

4 N. Govind, M. Petersen, G. Fitzgerald, D. King-Smith and J. Andzelm, *Comp. Mater. Sci*., 2003, **28**, 250–258.

5 S. Chen, S. Perathoner, C. Ampelli, C. Mebrahtu, D. Su and G. Centi, *Angew. Chem., Int. Ed*., 2017, **56**, 2699–2703.

6 Q. Liu, X. Zhang, B. Zhang, Y. Luo, G. Cui, F. Xie and X. Sun, *Nanoscale*, 2018, **10**, 14386–14389.

7 L. Hu, A. Khaniya, J. Wang, G. Chen, W. E. Kaden and X. Feng, *ACS Catal.*, 2018, **8**, 9312–9319.

8 X. Xiang, Z. Wang, X. Shi, M. Fan and X. Sun, *ChemCatChem*, 2018, **10**, 4530–4535.

9 G. Chen, X. Cao, S. Wu, X. Zeng, L. Ding, M. Zhu and H. Wang, *J. Am. Chem. Soc*., 2017, **139**, 9771–9774.

10 L. Zhang, X. Ji, X. Ren, Y. Ma, X. Shi, Z. Tian, A. M. Asiri, L. Chen, B. Tang and X. Sun, *Adv. Mater*., 2018, **30**, 1800191.

11 X. Li, T. Li, Y. Ma, Q. Wei, W. Qiu, H. Guo, X. Shi, P. Zhang, A. M. Asiri, L. Chen, B. Tang and X. Sun, *Adv. Energy Mater.*, 2018, **8**, 1801357..

12 R. Zhang, X. Ren, X. Shi, F. Xie, B. Zheng, X. Guo and X. Sun, *ACS Appl. Mater. Interfaces*, 2018, **10**, 28251–28255.

13 X. Zhang, Q. Liu, X. Shi, A. M. Asiri, Y. Luo, T. Li and X. Sun, *J. Mater. Chem. A*, 2018, **6**, 17303–17306.

14 Y. Zhang, W. Qiu, Y. Ma, Y. Luo, Z. Tian, G. Cui, F. Xie, L. Chen, T. Li and X. Sun, *ACS Catal.*, 2018, **8**, 8540–8544.

15 K. Jia, Y. Wang, Q. Pan, B. Zhong, Y. Luo, G. Cui, X. Guo and X. Sun, *Nanoscale Adv*., 2018, DOI: 10.1039/C8NA00300A.

16 Z. Wang, F. Gong, L. Zhang, R. Wang, L. Ji, Q. Liu, Y. Luo, H. Guo, Y. Li, P. Gao, X. Shi, B. Li, B. Tang and X. Sun, *Adv. Sci*., 2018, **5**, 1801182.

17 X. Wu, L. Xia, Y. Wang, W. Lu, Q. Liu, X. Shi and X. Sun, *Small*, 2018, **14**, 180311.

18 L. Zhang, X. Ren, Y. Luo, X. Shi, A. M. Asiri, T. Li and X. Sun, *Chem. Commun*., 2018, **54**, 12966–12969.

19 L. Ji, X. Shi, A. M. Asiri, B. Zheng and X. Sun, *Inorg. Chem*., 2018, **57**, 14692–14697.

20 Y. Wang, K. Jia, Q. Pan, Y. Xu, Q. Liu, G. Cui, X. Guo and X. Sun, *ACS Sustainable Chem. Eng.,* 2018, DOI: 10.1021/acssuschemeng.8b05332.